Journal of
Materials Chemistry A

Accepted Manuscript

This article can be cited before page numbers have been issued, to do this please use: A. Kong, C. Mao, Y. Wang, Q. Lin, X. Bu and P. Feng, *J. Mater. Chem. A*, 2016, DOI: 10.1039/C6TA00154H.

This is an *Accepted Manuscript*, which has been through the Royal Society of Chemistry peer review process and has been accepted for publication.

Accepted Manuscripts are published online shortly after acceptance, before technical editing, formatting and proof reading. Using this free service, authors can make their results available to the community, in citable form, before we publish the edited article. We will replace this *Accepted Manuscript* with the edited and formatted *Advance Article* as soon as it is available.

You can find more information about *Accepted Manuscripts* in the Information for Authors.

Please note that technical editing may introduce minor changes to the text and/or graphics, which may alter content. The journal's standard Terms & Conditions and the Ethical guidelines still apply. In no event shall the Royal Society of Chemistry be held responsible for any errors or omissions in this *Accepted Manuscript* or any consequences arising from the use of any information it contains.

ROYAL SOCIETY OF CHEMISTRY

www.rsc.org/materialsA

View Article Online
DOI: 10.1039/C6TA00154H

Journal of Materials Chemistry A

ARTICLE

Hierarchically Porous Few-layer Porphyrinic Carbon Nanosheets Formed by VO_x-Templating Method for High-Efficiency Oxygen Electroreduction

Received 00th January 20xx,
Accepted 00th January 20xx

DOI: 10.1039/x0xx00000x

www.rsc.org/

A. Kong [a,b],* C. Mao[a], Y. Wang[a], Q. Lin[a], X. Bu[c],* and P. Feng[a]*

Abstract A new vanadium oxide-templating synthesis strategy is used to synthesize porous few-layer porphyrinic carbon nanosheets (PPCNs) with highly efficient electrocatalytic activity for oxygen reduction reaction (ORR). Fe-porphyrin precursors were intercalated into V_2O_5 layers and directly transformed to carbon nanosheets after pyrolysis. Highly accessible porphyrinic Fe-N_4 moieties embedded within few-layer carbon nanosheets with hierarchical porosity and high surface area (1600 $m^2 g^{-1}$) were obtained. The PPCNs were demonstrated as the excellent non-precious metal catalysts for ORR in both alkaline and acidic media. Specifically, the PPCNs exhibited more positive half-wave potential than commercial Pt/C (20 wt%) in alkaline medium at the lower catalyst loading. Moreover through further pyrolysis treatment, the catalytic activity and durability of PPCNs for ORR in both media could be further improved. The novel synthetic method presented here opens up a new route for creating novel carbon nanomaterials for various applications.

1 Introduction

Carbon nanomaterials have attracted considerable attention because of their diverse applications including chemical sensing, adsorption and separation, catalysis, energy conversion and storage.[1-6] Various synthesis strategies have been developed to obtain carbon nanomaterials with desired morphologies such as nanotubes,[7] graphene,[8] and porous carbons.[9] One unique synthesis method is the hard-template approach based on inorganic host materials.[9, 10] With this method, carbon materials with high surface area, tunable pore structures, different morphologies, and high degree of graphitization can be obtained by annealing organic precursors in the confined space or local surroundings of hard templates such as SiO_2,[10-14] Al_2O_3,[15] MgO,[16-18] ZnO,[19, 20] and various molecular sieves.[9, 21, 22] V_2O_5 is known to easily form intercalation compounds.[23-26] Different organic guests can be dispersed and confined between the layers of V_2O_5 at the molecule level, and thermal conversion of such intercalation compound may be developed as a new reactive-template route for the preparation of unique carbon materials such as few-layer nanosheets. The reactive VO_x templates may provide a confined but connected local space for the formation of a three-dimensional (3-D) nanosheet structure. Moreover, the oxidation-reduction reaction between V_2O_5 and organic precursors could create more pore structures in the carbon nanosheet and expose more carbon edges, which is crucial for the preparation carbon-based catalysts and adsorbents. Furthermore, organic precursors with designed functional groups and different contents could provide the additional uniformity and abundant tunability for the preparation of carbon materials with the targeted functions. However, as so far, there are few reports about the successful synthesis of functional carbon materials by VO_x-templating method.

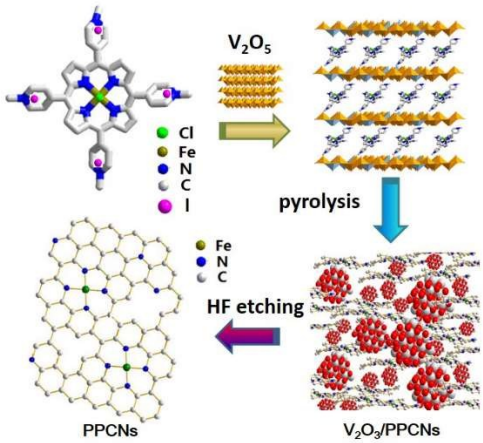

Fig. 1. An illustration of the synthesis of porous porphyrinic carbon nanosheets (PPCNs) from iron (III) meso-tetra (N-methyl-4-pyridyl) porphyrin tetra-iodide (FeTMPyPI).

Due to the high chemical and mechanical stability, excellent electron transport, and environmentally friendly properties, carbon nanomaterials can be widely utilized as electrode materials, such as eletrocatalysts for ORR. Currently, the development of efficient, durable, and low-cost alternatives to Pt-based electrocatalysts is still a great challenge for the large-scale commercialization of fuel cells.[27] Doping of iron and nitrogen into carbon (Fe-N-C) has been shown to be a promising route for making efficient non-precious metal catalysts (NPMCs).[28] A typical example is the pyrolysis of metal macrocycle compounds supported on carbon materials. Theoretical and experimental studies suggested that the Fe-N_4 moieties

[a] School of Chemistry and Molecular Engineering, East China Normal University, 500 Dongchuan Road, Shanghai 200241, P.R.China.
[b] Department of Chemistry, University of California, Riverside, California 92521, United States
[c] Department of Chemistry and Biochemistry, California State University, Long Beach, California 90840, United States.
Electronic Supplementary Information (ESI) available: [details of any supplementary information available should be included here]. See DOI: 10.1039/x0xx00000x

embedded in graphitic carbon were highly efficient active sites for ORR in a wide range of pH.[29-35] Even though Fe-N_4-porphyrin compounds are known as precursors in the preparation of Fe-N_4-embedded carbons, the simple pyrolysis of Fe-N_4-containing porphyrins or carbon-supported Fe-N_4-macrocycles usually results in the formation of carbons with difficult-to-control morphology, low surface area, and insufficient activity for ORR.[35, 36] It is desirable to prepare Fe-N-C nanomaterials with controllable morphology, highly accessible Fe-N_4 moieties, and high surface area for ORR applications.

Herein, we successfully develop a reactive vanadium oxide-templating strategy for the synthesis of Fe-N-C nanosheets (Fig. 1), in which Fe-N_4-porphyrin compounds are directly converted into hierarchical porous porphyrinic Fe-N-C (assigned to PPCNs) for the first time. The Fe-N_4-porphyrin compounds containing abundant carbon, nitrogen and Fe are especially chosen serving as the only precursor of PPCNs.[29-35, 37] Vanadium oxides are used as reactive hard templates and nanoreactors, which provide a specially confined but interlinked space for directly converting Fe-N_4-porphyrin into hierarchical porous Fe-N-C nanosheets. By this novel route, the obtained PPCNs possess unique porosity and high surface area up to 1600 $m^2\ g^{-1}$ bestowing the materials with efficient adsorptive and transporting properties. With the embedded active Fe-N_4 sites on the surface of PPCNs, this newly synthesized few-layer Fe-N-C materials demonstrate high efficient catalytic activity for ORR in both alkaline and acidic media.

2 Experimental

2.1 Synthesis

2.1.1 Synthesis of iron (III) meso-tetra(N-methyl-4-pyridyl) porphyrin tetra-iodide (FeTMPyPI)

The porphyrin compounds were prepared according to the reported synthesis route.[35] In a typical synthesis, 2.0 g of meso-tetra(4-pyridyl) porphyrin (TPyP) and 5.0 g of $FeCl_3•6H_2O$ were added in 100 mL of ethanol, and this mixtures were refluxed for 24 h. The resulting FeTPyP samples were separated by filtering, and were washed with anhydrous ethanol to remove residual $FeCl_3•6H_2O$. For the methylation of FeTPyP, the resultant FeTPyP and 7.2 g of methyl iodide (CH_3I) were refluxed at 120 °C in 100 mL N, N-dimethylformamide (DMF) for 24 h. After cooled to room temperature, 200 mL of acetone was added in the mixture above. The FeTMPyPI products were collected by filtering and washing with a large amount of acetone and dried in vacuum oven at 60 °C.

2.1.2 Synthesis of PPCNs

PPCNs were prepared by thermal conversion of the FeTMPyP/V_2O_5 intercalation compounds. In a typical synthesis, 1.0 g of FeTMPyPI was added into 150 mL deionized water and stirred for 1h at room temperatures. After that, 2.0 g of commercial V_2O_5 powders was added into the above solution. The mass ratio of FeTMPyP to V_2O_5 is 1:2. The resultant suspension was heated and acutely refluxed for 72 h in a flask equipped with condenser pipe. The green FeTMPyP/V_2O_5 interaction compounds were collected by hot filtration and washed by water and ethanol. The dried FeTMPyP/V_2O_5 compounds were heated at 750 °C for 4 h in argon, with a heating rate of 5 °C min^{-1}. Finally, PPCNs were obtained after the removal of vanadium oxides by acid etching (HF, 5 wt%). For the second pyrolysis treatment of PPCNs, the as-prepared PPCNs were heated at 700 °C for 4h in argon, with a heating rate of 5 °C min^{-1}. The resultant material was assigned to PPCN-700

2.2 Characterization

A JEM-2010 transmission electron microscope and a Hitachi ST-4800 scanning electron microscope (SEM) were used to observe the morphology and local structure of carbon materials. Powder X-ray diffraction patterns (XRD) were obtained on a D8 Advance (Bruker AXS, Germany) diffractometer with CuKα radiation (40 kV, 40 mA). N_2 adsorption/desorption measurements were measured at 77 K on a Micromeritics ASAP 2020 analyzer. X-ray photoelectron spectroscopy (XPS) measurements were carried out on Axis Ultra DLD using Al Kα radiation with C 1s (284.8 eV) as a reference to correct the binding energy. The Fourier-transform infrared spectroscopy (FT-IR) was performed on the NICOLET 6700 (Thermo) infrared spectrometer. The measurement of ultraviolet visible (UV-VIS) diffuse reflectance spectrum was carried out on UV-3101PC (SHIMADZU) spectrometer. The atomic force microscope (AFM) images of graphene sample are obtained by Vecco multimode+ Dimension3100+ NanoScope 3D on a mica plate substrate, operating in tapping mode.

The electrocatalytic activities of as-prepared PPCNs for ORR were evaluated by cyclic voltammetry (CV), rotating disk electrode (RDE) and ring-rotated disk electrode (RRDE) techniques. A standard three electrode cell was used including a working glass carbon RDE (Pine, 5.0 mm) or RRDE (Pine, 5.6 mm), an Ag/AgCl, KCl (3 M) electrode as reference electrode, and a Pt electrode as counter electrode. The experiments were carried out in O_2-saturated 0.1 M KOH and 0.1 M $HClO_4$ solution. The working electrodes were prepared through dispersing 10 mg of PPCNs in 1.28 ml alcohol solution containing 80 µL of a 5 wt% Nafion solution by sonication. Catalyst suspension was pipetted onto a polished glassy carbon electrode surface and the electrode was dried at room temperature. A commercially available 20 wt% Pt/C catalyst obtained from JM Company was used for comparison. The general loading of active PPCNs on the working electrode is 0.25 mg cm^{-2} in 0.1 M KOH and 0.60 mg cm^{-2} in 0.1 M $HClO_4$ solutions. The catalyst loading of Pt/C on the electrode is 0.1 mg (Pt-C) cm^{-2} in both electrolyte. All the potentials are corrected to the reversible hydrogen electrode (RHE) potentials ($E_{RHE}=E_{Ag/AgCl}$ +0.973 in 0.1 M KOH, $E_{RHE}=E_{Ag/AgCl}$ +0.293 in 0.1 M $HClO_4$). The ORR current is obtained by subtracting the current measured in Ar-saturated electrolytes from the current measured in O_2-saturated electrolytes.

The HO_2- percentage and the corresponding electron number (n) transferred during the ORR were calculated by the following equations:

$$n = \frac{4I_D}{I_D + I_R/N}\ ; \quad \%HO_2^- = 200 \times \frac{I_R/N}{I_D + I_R/N}$$

, where I_D, I_R and N= 0.37 are the disk current, ring current and collection efficiency, respectively for the employed RRDE.

3 Results and discussion

As shown in Fig. 1, PPCNs were obtained through the heat-treatment of composite FeTMPyP/V_2O_5 intercalation compounds. The key step for the synthesis of the FeTMPyP/V_2O_5 intercalation compound was to introduce FeTMPyPI with bigger molecule size (about 1.7 nm) into the layers of V_2O_5 powder. The reaction between V_2O_5 and I^- in a boiling aqueous solution caused V_2O_5 to undergo a reductive layer reconstruction, which successfully lead to the formation of FeTMPyP/V_2O_5 intercalation compound.[23, 38] The deconvoluted V 2p XPS spectrum of FeTMPyP/V_2O_5 verified that V(Ⅴ) atoms in V_2O_5 layers were partly reduced into V(Ⅳ) by I^- (Fig. S1), which was also supported by the observation of purple iodine

crystals. After FeTMPyP was intercalated, the $d_{(001)}$ distance of V_2O_5 (JSPDF #41-1426) changed from 0.43 nm to 1.25 nm in FeTMPyP/V_2O_5 compounds (Fig. 2 a and b). The molecule size of FeTMPyP cations is much larger than 0.82 nm. The FeTMPyP cations should be intercalated into the layers with a tilt angle in the monolayer, similar to the reported V_2O_5 intercalation compounds.[23, 38, 39] TEM images showed that orange V_2O_5 particles with the particle size of 1-15 μm (Fig. S2) were transformed into silk-like dark green FeTMPyP/V_2O_5 composites (Fig. 3 A). A closer observation for lattice fringes by high-resolution TEM (Fig. 3 B, inset) showed that the lattice spacing (about 1.3 nm) corresponded to the (001) plane of the intercalation compounds. The Fourier-transform infrared spectroscopy (FT-IR) spectrum (Fig. S3), elemental analysis results (C, 13.05 wt%; N, 2.82 wt%) and the deconvoluted XPS spectra for V, Fe, C, N (Fig. S2) further confirmed the formation of FeTMPyP/V_2O_5 intercalation compounds.

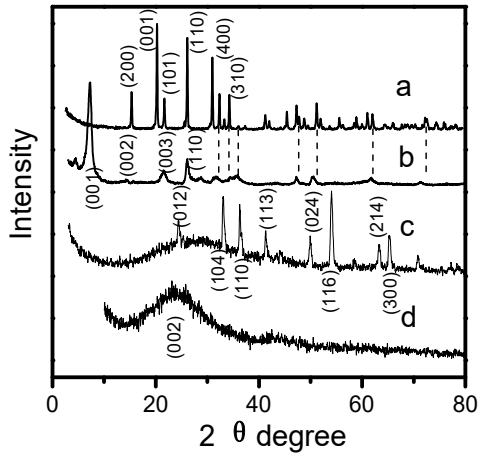

Fig. 2. XRD patterns of commercial V_2O_5 (a), FeTMPyP/V_2O_5 intercalation compounds (b), V_2O_3 and carbon materials obtained by heating FeTMPyP/V_2O_5 at 750 °C for 4 h (c), and the prepared PPCNs (d).

After the FeTMPyP/V_2O_5 intercalation compounds were treated in argon at 750 °C for 4 h, the carbonization of FeTMPyP in the interlayer regions of V_2O_5 and the reduction of lamellar V_2O_5 to rhombohedral V_2O_3 particles occurred simultaneously, leading to the formation of the composites of V_2O_3 nanoparticles and Fe-N-C nanosheets. The presence of V_2O_3 was verified by XRD (Fig. 2 c, JSPDF# 34-0187). The TEM of this thermal decomposition product (Fig. 3 C) showed that numerous V_2O_3 particles with the size of 3-300 nm were embedded between or on the formed Fe-N-C sheets. A major concern in vanadium-oxide-templating method is the low yield of Fe-N-C materials with considerable impurities of vanadium nitrides and carbides formation. In this work, the formation of vanadium nitrides (VN_x) or carbides was prevented by annealing FeTMPyP/V_2O_5 under the optimized heat-treatment temperatures (<750 °C) (Fig. 2 c and Fig. S4) and the proper use of V_2O_5 to porphyrin ratio in the intercalation compounds. After etching off V_2O_3 with HF (5 wt% aqueous solution), PPCNs with a yield of about 25 % (based on the intercalated porphyrin) were obtained (Fig. 2 d).

Both TEM and SEM images indicate a few-layer nanosheet morphology of PPCNs (Fig. 3 D and F). The length of nanosheets is about 1-2 μm, while the thickness estimated by atomic force microscope is about 0.5-6 nm (Fig.S5). Unlike the stacked Fe-N-C sheets reported previously, these few-layer nanosheets are crosslinking and tend to form a 3-D open structure. The reason may be that vanadium oxides are reactive and easily converted. The FeTMPyP carbon precursors in different vanadium oxide layers have not been completely isolated and can move and connect each other in the carbonization. HRTEM (Fig. 3E) revealed discontinuous graphitic lattices of PPCNs, in agreement with the observed SAED rings. The graphitization degree of the prepared PPCN was lower than typical graphene carbon. The XRD of few-layer PPCNs revealed two broad peaks at 2θ 24 and 43°, assigned to the degree of stacking order of the layered carbon structure (002) and ordered hexagonal carbon structure (100), respectively.[22] The broadness of the XRD peaks was contributed to the random stacking of thin corrugated nanosheets and nano-sized carbon grains with lower crystallization degree.[22] The Raman spectrum of PPCNs (Fig. S6) exhibited two peaks at about 1367 and 1593 cm^{-1}, corresponding to the well-defined D and G bands of carbon, [40, 41] respectively. The D to G peak intensity ratio was about 0.9. There is a distinguishable broad 2D peak centered at 2780 cm^{-1}. These results indicated that this PPCN was few-layer nanosheets with abundant defects or disordered structures. [40, 41]

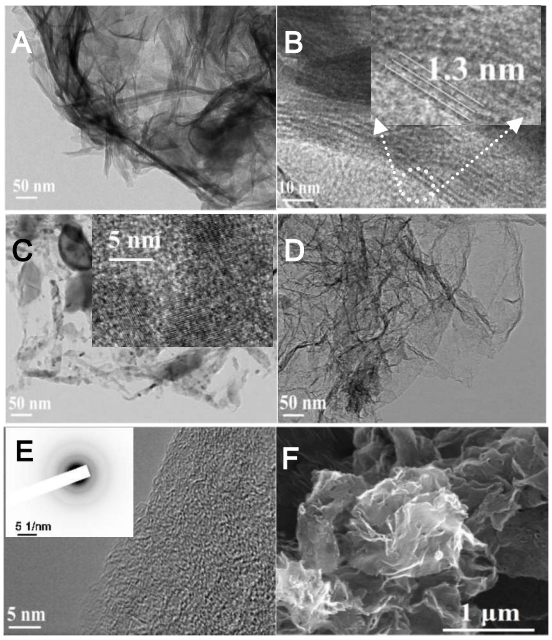

Fig. 3. TEM and HRTEM images for FeTMPyP/V_2O_5 intercalation compounds (A and B), the composites of V_2O_3 and PPCNs obtained by heating FeTMPyP/V_2O_5 at 750 °C for 4 h (C), and PPCNs (D and E). Inset in (E) is the select area electron diffraction (SAED) image. (F) SEM image for PPCNs

Previously, the Fe-N-C nanosheets typically prepared by the pyrolysis of graphene oxide-supported different precursors[29, 42, 43] often showed the relatively low surface area.[44] Many active Fe-N_x sites for ORR were buried into the closed carbon layers. Impressively this Fe-N-C nanosheets synthesized here possessed a Brunauer-Emmett-Teller (BET) surface area of 1600 $m^2\ g^{-1}$ (Fig. S7 A), (mesopore surface area of 1228 $m^2\ g^{-1}$ and a micropore surface area of 372 $m^2\ g^{-1}$), much higher than previously reported nanosheets.[45-47] The pore size distribution curves for PPCNs revealed several hierarchical pores centered at around 1.1, 3.4, 20, and 45 nm (Fig. 4 and S7). The carbonization of porphyrins in confined space of

reactive vanadium oxides might contribute to the formation of micropores in nanosheets, while the removal of V_2O_3 nanoparticles may have created meso- and even macropores in or between the nanosheets. Hierarchical porosity and 3-D open nanostructures contributed to the highly accessible surface area of PPCNs and the easy access to Fe-N_4 active sites, which facilitated the facile infiltration of electrolyte and fast transport of O_2 in the nanosheets. Such PPCNs also exhibit a high uptake of CO_2 at 273 K and 1 atm (74 $cm^3\ g^{-1}$), which is even higher than that of the highly porous ZIF-69 metal-organic framework (70 cm^3g^{-1}) under the same conditions (Fig.S7 D).[48]

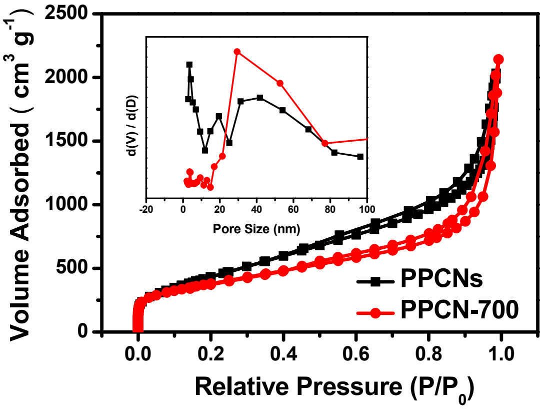

Fig. 4 N_2 adsorption-desorption isothermal curves for PPCNs and PPCN-700 and the corresponding mesopore size distribution curves obtained by BJH method on the basis of adsorption branch.

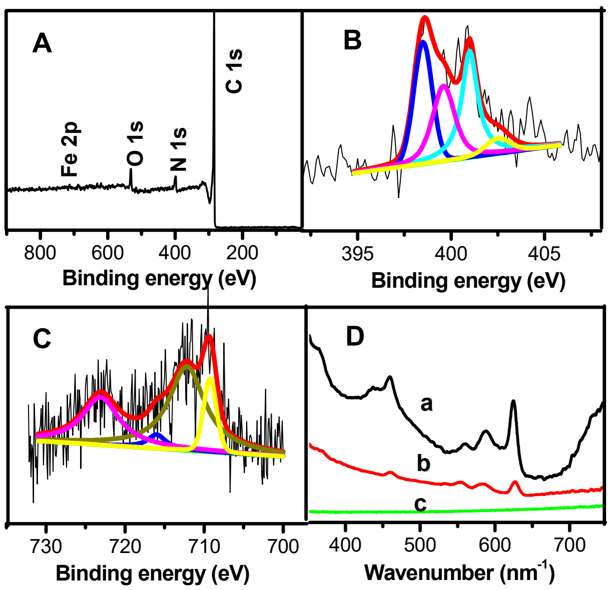

Fig. 5. XPS survey spectrum (A) and the deconvoluted N1s (B) and Fe 2p (C) XPS spectra of PPCNs. The UV-Vis diffuse reflectance spectra (D) of FeTPyP porphyrin (a), PPCNs (b), and commercial active carbons(c).

High density and turnover number of active sites are desirable features of efficient catalytic materials.[1, 49-51] The uniform distribution of Fe and N in PPCNs observed by elemental mapping images of energy dispersive spectroscopy (SEM-EDS) contributed to the efficient use of active sites (Fig. S8). The XPS survey spectrum indicated that about 5.1 at% nitrogen (5.5 wt% in bulk determined by element analysis) and 0.35 at% Fe were embedded on the surface of PPCNs (Fig. 5 A). The pyrolysis of porphyrin compounds can often derive porphyrinic carbons with Fe-N_4 moieties in the framework.[28, 30] Fe 2p 3/2 XPS peak of the prepared PPCNs has binding energy of 710-712 eV (Fig. 5 C), similar to that of Fe 2p 3/2 XPS in FeTPyPI precursors (Fig.S1 and S9). It indicated that the Fe atoms may belong to the N-coordinated Fe ions, similar to the reported results by Hashimoto.[52] The N peak at 399.6 eV in the deconvoluted N1s XPS spectrum could be mainly ascribed to Fe-coordinated nitrogen atoms [52, 53] (probably containing pyrrolic-like nitrogen atoms) in the carbon frameworks (Fig. 5 B). Other N peaks could originate from pyridinic (at 398.3 eV), graphitic (at 401.5 eV) and oxidized type of (at 403.6 eV) nitrogen atoms, respectively.[54] Moreover, an infrared band at around 2650 cm^{-1} corresponding to C-N vibration (Fig. S3 d) and four typical ultraviolet visible (UV-VIS) diffuse reflectance peaks (Fig. 5 D) corresponding to porphyin-like materials could also be observed.[53] These results indicated that considerable porphyrinic Fe-N_4 moieties were successfully embedded on the surface of PPCNs.

The electrocatalytic activity of PPCNs in 0.1 M KOH alkaline electrolyte is very impressive. The corresponding CV curves in Ar- or O_2-saturated 0.1 M KOH solutions confirmed that the reduction currents at the peak potential of 0.85 V resulted from the electrocatalytic ORR over PPCNs (Fig. S10 A). After the subtraction of capacitive currents from the ORR currents, the RDE polarization curves of PPCNs at 1600 rpm showed the same ORR half-wave ($E_{1/2}$) potential (0.82 V) and current density (i.e. about 5.0 mA cm^{-2} at 0.5 V) as commercial Pt/C (20 wt%, JM) catalysts (Fig. S11A). This result was achieved with the same catalyst loading amount on the electrodes (0.1 mg cm^{-2}) to the commercial Pt/C catalysts. When increasing the catalyst amount of PPCNs to 0.25 mg cm^{-2}, more positive ORR $E_{1/2}$ potential (0.84 V) can be obtained (Fig. 6 A). This $E_{1/2}$ value is about 5-10 mV more positive than other porphyrin-derived materials and is among the excellent ORR electrocatalysts in basic medium.[42, 53, 55, 56] Over 0.25 mg cm^{-2} catalyst loading of PPCNs on the electrodes caused a thick catalyst layers and a waste of inner layer catalyst (Fig.S11A), although the $E_{1/2}$ value could still be slightly improved. With a relatively lower catalyst loading, high ORR current density and low overpotential in alkaline medium indicate a high catalytic activity of such PPCNs for ORR.

Moreover, this PPCN was also shown as the efficient ORR electrocatalyst in 0.1 M $HClO_4$ electrolyte (Fig. S10 B). The PPCN electrode with a catalyst loading of 0.60 mg cm^{-2} showed an $E_{1/2}$ value of 0.74 V, about 80 mV more negative than that of Pt/C electrocatalyst (0.1 $mg_{(Pt-C)}$ cm^{-2}). However, it had a higher diffusion-limiting current density than Pt/C catalyst below 0.5 V (Fig. 6 B), indicate its efficient catalytic activity of such PPCNs for ORR. The high ORR catalytic performance of PPCNs in a broad pH media could be attributed to the synergetic effects of highly accessible surface, high density of ORR active sites including Fe-N_4, graphitic N and pyridinic N, and exposed carbon edges,[28] and appropriate graphitization degree of PPCNs.

We also studied the use of TMPyPI and CoTMPyPI as precursors for the synthesis of metal-free or Co-N_4 moieties-embedded PPCNs by the similar synthesis route (Fig. S12). However, VN_x particles were easily produced during the thermal conversion of CoTMPyP/V_2O_5 even at lower temperatures such as 675 °C. The formation of VN_x would generally consume active nitrogen ingredients in the surface of PPCNs. The ORR activities of these PPCNs are respectable but lower than that of PPCNs obtained from FeTMPyPI at the same temperatures in both acidic and alkaline electrolytes (Fig. S13), in

terms of their $E_{1/2}$ values and current densities. It suggested a remarkable effect of metal center in porphyrin precursors on the ORR activity of the resultant PPCNs, and Fe-N_4 sites in carbon framework often show higher activity for ORR than Co-N_x sites. [28, 57]

The mass ratio of FeTMPyPI to V_2O_5 in the preparation of intercalation compounds is another important factor that could impact the activity of the formed PPCNs. When the mass ration of FeTMPyP to V_2O_5 changed from 1:3, 1:2 to 1:1, the prepared intercalation compounds showed the similar XRD patterns and $d_{(001)}$ values. This result suggested that the increasing FeTMPyP may be continuously interacted into the same layers of V_2O_5 in the monolayer. After underdoing the thermal conversion of these interaction compounds, the carbon materials with the similar nanosheet morphology were obtained. It is noticed that VN_x is easily formed when the mass ration of FeTMPyP to V_2O_5 is over 1:1. In consideration of the yield, purity, and the ORR activity of the resultant PPCNs, the mass ratio of FeTMPyPI to V_2O_5 of 1:2 is appropriate (Fig. S14).

The ORR activity of the prepared PPCNs is sensitive to the heat-treatment temperature of the composite porphyrin/V_2O_5. High temperature tended to give VN_x in the products and reduced the ORR activity of the corresponding PPCNs (Fig.S4 and S15). However, a lower pyrolyzation temperature would be detrimental to the graphitization of PPCNs. The best PPCN for ORR is the sample prepared by heating FeTMPyP/V_2O_5 at 750 °C as described above.

The as-prepared PPCNs were further treated at 700 °C for 4h (PPCN-700) to enhance the catalytic performance for ORR. The characterization results by XRD, SEM, N_2-sorpotion, TEM, and XPS (Fig.4, S16 and S17) show that PPCN-700 still has a similar few-layer nanosheet morphology but with a remarkably higher degree of graphitization after undergoing the second pyrolysis treatment. High-resolution TEM and SAED measurement for several carbon grains showed the clear graphite lattices or diffraction ring. It still has a hierarchical porous structure, although the pore distribution has changed and the total BET surface area decreased to 1357 $m^2\ g^{-1}$. The XPS revealed the decreasing of oxygen content and the increasing of nitrogen content (6.8 at%) on the surface of PPCN-700, suggesting a repair effect of carbon surface during the second pyrolysis treatment. As a result, the PPCN-700 exhibited the improved activity for ORR. The PPCN-700 electrodes showed the ORR $E_{1/2}$ of 0.85 V in 0.1 M KOH and 0.75 V in 0.1 M $HClO_4$, about 10 mV more positive than PPCNs in both electrolytes.

The kinetic reduction process of O_2 on highly active PPCNs was also investigated. Two-electron reduction of oxygen is generally less desirable due to the low efficiency and the corrosive nature of the resulting hydrogen peroxide. The numbers of electrons transferred during the ORR over PPCNs in both electrolytes were calculated to be 3.90-3.95 in the potential range of 0.6 to 0.2 V based on the investigated RRDE results (Fig. 6 C). For the ORR over PPCN-700, the calculated electron numbers even are closer to theoretical 4 electrons (3.95-4.00), similar to the Pt/C electrocatalysts. These results confirm that PPCNs and PPCN-700 can efficiently catalyze the reduction of oxygen in a nearly direct four-electron process in both alkaline and acidic media ($O_2+2H_2O+4e=4OH^-$ in 0.1 M KOH; $O_2+4H^++4e=2H_2O$ in 0.1 M $HClO_4$[30, 58]). Moreover, the PPCNs reported here clearly showed superior durability during the ORR in both media, in comparison with Pt/C catalysts. A relative ORR current of 91 % on the PPCN electrodes in 0.1 M KOH (Fig. 6 E) and 85 % in 0.1 M $HClO_4$ (Fig. 6 F) solution still remained after 20,000s. In comparison, about 75 and 70 % ORR currents on Pt/C electrodes were detected after 10,000s in 0.1 M KOH and in 0.1 M $HClO_4$ solution, respectively, owing to the easily poisoned property of Pt. [59] The ORR peak currents and capacitive currents in the CVs over PPCNs were not significantly changed (Fig. S18) after 5, 000 cycles in both electrolytes. Furthermore, the second heat-treatment for PPCNs were found to remarkably enhance the durability during ORR. A relative ORR current of 98 % on the PPCN-700 electrodes in 0.1 M KOH and 91 % in 0.1 M $HClO_4$ solution can be maintained after 50,000s. Better durability of PPCN-700 should be attributed to the improved degree of graphitization and lower H_2O_2 yield of PPCN-700

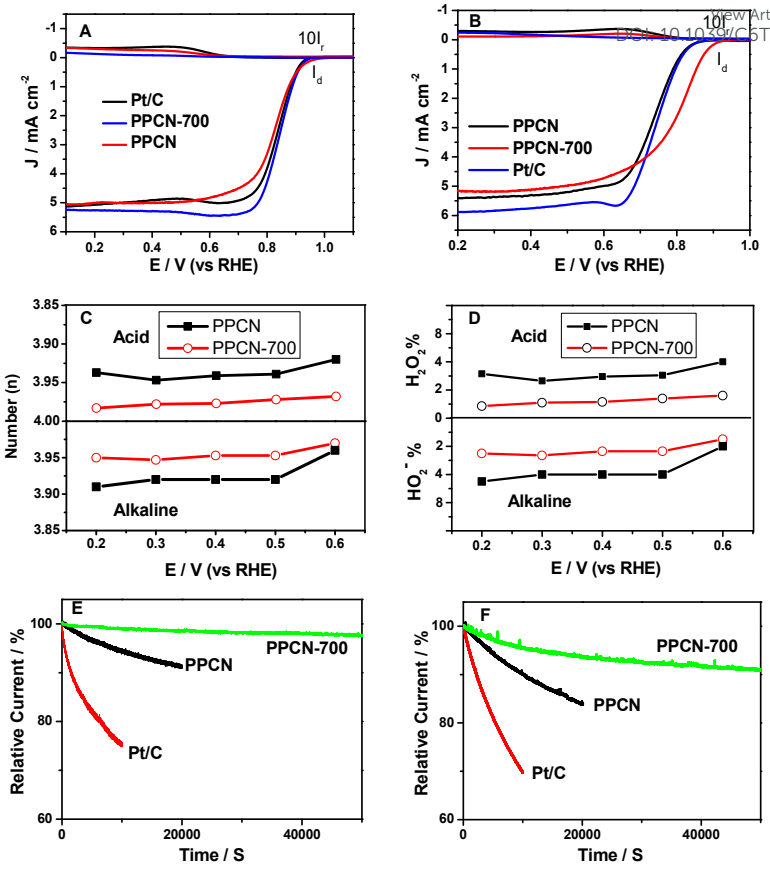

Fig 6. (A and B) RRDE polarization curves on PPCNs and commercial Pt/C (20 wt%) in 0.1 M KOH (A) and 0.1 M $HClO_4$ (B) electrolytes at 1600 rpm; (C and D) The ORR electron transferred number (n) and yield of H_2O_2 (%) of different catalysts based on the corresponding RRDE polarization curves. The catalyst loadings of PPCNs on the RRDE electrodes in 0.1 M KOH and 0.1 M $HClO_4$ electrolytes are 0.25 and 0.60 mg cm^{-2}, respectively. The scan rate is 5 mV s^{-1}. (E and F) Current–time (i–t) chronoamperometric response of PPCNs and Pt/C at 0.55 V in O_2-saturated 0.1 M KOH (E) and 0.1 M $HClO_4$ (F) at a rotation rate of 1600 rpm on the RDE electrode with a catalyst loading of 0.25 mg cm^{-2}, respectively. The catalyst loading of Pt/C is 0.1 mg (Pt/C) cm^{-2} in all the testing.

(about < 3% in both electrolytes, Fig. 6 D). In addition, like other non-precious metal catalyst, PPCN materials also revealed better methanol tolerance. As testified by RDE polarization curves in different electrolytes (shown in Fig. S19), there are no notable changes in the ORR $E_{1/2}$ and current density over PPCNs in the presence of methanol (2 wt%).

4 Conclusions

In summary, few-layer porphyrinic carbon nanosheets were successfully prepared by a reactive "vanadium oxide-templating" synthesis strategy. Vanadium oxides not only serve as hard templates or supports but also provide a unique local environment for producing such nanosheet materials. Thermal conversion of porphyrins confined between the layers of V_2O_5 directly created the few-layer Fe-N-C naonosheets with hierarchical porosity and highly accessible surface. Active porphyrin-like Fe-N_4 moieties for ORR are shown to embed on the surface of such nanosheets with appropriate degree of graphitization. The integration of these desirable features led to highly efficient ORR activity that is comparative (in alkaline medium) or comparable to (in acidic medium) commercial Pt/C (20 wt%) catalysts. Furthermore, the second pyrolysis treatment are effective in increasing the graphitization degree of PPCN and further improving its activity and durability for ORR. This VO_x-templated synthesis method opens up a novel pathway for the preparation of highly accessible carbon nanosheets with hierarchical porosity and exceptional electrocatalytic performance. The obtained PPCN materials represent the promising cathode catalysts for ORR in fuel cell applications.

Supporting Information. N_2-sorption analyses, FT-IR, TEM, XPS, AFM and SEM-EDS spectra for the precursors and different PPCNs as well as the ORR activity and durability for different PPCNs are available free of charge via the Internet at http://pubs.acs.org.

*Corresponding Author

Aiguo Kong; School of Chemistry and Molecular Engineering, East China Normal University, 500 Dongchuan Road, Shanghai 200241, P.R.China, E-mail: agkong@ chem.ecnu.edu.cn.

Pingyun Feng; Department of Chemistry, University of California, Riverside, CA 92521, E-mail: pingyun.feng@ucr.edu.

Xianhui Bu; Department of Chemistry and Biochemistry, California State University, Long Beach, CA 90840, E-mail: xianhui.bu@csulb.edu.

Acknowledgements

This work is mainly supported by the U.S. Department of Energy, Office of Basic Energy Sciences, Division of Materials Sciences and Engineering under Award # DE-FG02-13ER46972 (Feng). Dr. Kong thanks the financial support from China Scholarship Council, National Natural Science Foundation (No. 21303058), Shanghai Municipal Natural Science Foundation (No. 13ZR1412400 and 11JC1403400) to Dr. Kong.

Notes and references

1 W. Qi and D. Su, *ACS Catal.*, 2014, **4**, 3212-3218.
2 H. Jin, H. Huang, Y. He, X. Feng, S. Wang, L. Dai and J. Wang, *J. Am. Chem. Soc.*, 2015,**137**,7588-7591.
3 Y. Xing, X. Zheng, Y. Wu, M. Li, W. H. Zhang and C. Li, *Chem. Commun.*, 2015, **51,** 8146-8148.
4 W. Lu, M. Bosch, D. Yuan and H. C. Zhou, *Chemsuschem*, 2015, **8**, 433-438.
5 C. Zhu, Y. Wen, P. A. Van Aken, J. Maier and Y. Yu, *Adv. Funct. Mater.*, 2015, **25**, 2335-2342.
6 Z. Y. Sui and B. H. Han, *Carbon*, 2015, **82**, 590-598.
7 R. Andrews, D. Jacques, D. Qian and T. Rantell, *Acc.Chem. Res.*, 2002, **35**, 1008-1017.
8 Y. Zhu, S. Murali, W. Cai, X. Li, J. W. Suk, J. R. Potts and R. S. Ruoff, *Adv. Mater.*, 2010, **22**, 3906-3924.
9 C. Liang, Z. Li and S. Dai, *Angew. Chem. Int. Ed.*, 2008, **47**, 3696-3717.
10 Y. Zhai, Y. Dou, D. Zhao, P. F. Fulvio, R. T. Mayes and S. Dai, *Adv. Mater.*, 2011, **23**, 4828-4850.
11 W. Li, D. Chen, Z. Li, Y. Shi, Y. Wan, G. Wang, Z. Jiang and D. Zhao, *Carbon*, 2007, **45**, 1757-1763.
12 X. Chen, Y.-S. Jun, K. Takanabe, K. Maeda, K. Domen, X. Fu, M. Antonietti and X. Wang, *Chem. Mater.*, 2009, **21**, 4093-4095.
13 Y. Wang, A. Kong, X. Chen, Q. Lin and P. Feng, *ACS Catal.*, 2015, **5**, 3887-3893.
14 S. Xia, N. Daems, B. Geboes, M. Kurttepeli, S. Bals, T. Breugelmans, A. Hubin, I. F. J. Vankelecom and P. P. Pescarmona, *Appl. Catal. B Environ.*, 2015, **176**, 212-224.
15 M. Golshadi, J. Maita, D. Lanza, M. Zeiger, V. Presser and M. G. Schrlau, *Carbon*, 2014, **80**, 28-39.
16 H. Wang, X. Sun, Z. Liu and Z. Lei, *Nanoscale*, 2014, **6**, 6577-6584.
17 S. Chen, J. Bi, Y. Zhao, L. Yang, C. Zhang, Y. Ma, Q. Wu, X. Wang and Z. Hu, *Adv. Mater.*, 2012, **24**, 5593-5597.
18 T. Morishita, T. Tsumura, M. Toyoda, J. Przepiorski, A.W. Morawski,H. Konno, M. Inagaki, *Carbon*, 2010, **48**,2690-2707.
19 P. Mbuyisa, S. P. Bhardwaj, F. Rigoni, E. Carlino, S. Pagliara, L. Sangaletti, A. Goldoni, M. Ndwandwe and C. Cepek, *Carbon*, 2012, **50**, 5472-5480.
20 K. S. Krishna, G. Vivekanandan, D. Ravinder and M. Eswaramoorthy, *Chem. Commun.*, 2010, **46**, 2989-2991.
21 Z. Yang, Y. Xia, X. Sun and R. Mokaya, *J. Phys. Chem. B*, 2006, **110**, 18424-18431.
22 W. Ding, Z. Wei, S. Chen, X. Qi, T. Yang, J. Hu, D. Wang, L.-J. Wan, S. F. Alvi and L. Li, *Angew. Chem.*, 2013, **125**, 11971-11975.
23 Y. Shan, R. H. Huang and S. D. Huang, *Angew. Chem. Int. Ed.*, 1999, **38**, 1751-1755.
24 A. Roy, M. Pradhan, C. Ray, R. Sahoo, S. Dutta and T. Pal, *CrystEngComm*, 2014, **16**, 7738-7744.
25 A. Kong, Y. J. Ding, P. Wang, H. Q. Zhang, F. Yang and Y. K. Shan, *J. Solid State Chem.*, 2011, **184**, 331-336.
26 F. J. Quites, C. Bisio, R. d. C. G. Vinhas, R. Landers, L. Marchese and H. O. Pastore, *J. Col. Inter. Sci.,* 2012, **368**, 462-469.
27 M. Liu, R. Zhang and W. Chen, *Chem. Rev.*, 2014, **114**, 5117-5160.
28. G. Wu and P. Zelenay, *Acc. Chem. Res.*, 2013, **46**, 1878-1889.
29. X. Fu, Y. Liu, X. Cao, J. Jin, Q. Liu and J. Zhang, *Appl. Catal. B: Envir.*, 2013, **130–131**, 143-151.
30. S. Kattel and G. Wang, *J. Phys. Chem. Lett.*, 2014, **5**, 452-456.
31. D. H. Lee, W. J. Lee, W. J. Lee, S. O. Kim and Y.-H. Kim, *Phys. Rev. Lett.*, 2011, **106**, 175502.
32. L. Wang, J. Yin, L. Zhao, C. Tian, P. Yu, J. Wang and H. Fu, *Chem Commun*, 2013, **49**, 3022-3024.
33. J. Yang, D.-J. Liu, N. N. Kariuki and L. X. Chen, *Chem Commun*, 2008, 329-331.
34. J. Zhang, Z. Wang and Z. Zhu, *J. Power Sources*, 2014, **255**, 65-69.
35. A. Kong, B. Dong, X. Zhu, Y. Kong, J. Zhang and Y. Shan, *Chem. Eur. J.*, 2013, **19**, 16170-16175.
36. H. Liu, Z. Shi, J. Zhang, L. Zhang and J. Zhang, *J. Mater. Chem.*, 2009, **19**, 468-470.
37. T. Li, Y. Peng, K. Li, R. Zhang, L. Zheng, D. Xia and X. Zuo, *J. Power Sources*, 2015, **293**, 511–518.

View Article Online
DOI: 10.1039/C6TA00154H

38. A. Bose, P. He, C. Liu, B. D. Ellman, R. J. Twieg and S. D. Huang, *J. Am. Chem. Soc.*, 2001, **124**, 4-5.
39. A. Vadivel Murugan, *J. Power Sources*, 2006, **159**, 312-318.
40. S. Some, Y. Kim, Y. Yoon, H. Yoo, S. Lee, Y. Park and H. Lee, *Sci. Rep.*, 2013, **3**, 1929
41. R. Hawaldar, P. Merino, M. R. Correia, I. Bdikin, J. Grácio, J. Méndez, J. A. Martín-Gago and M. K. Singh, *Sci. Rep.*, 2012, **2**, 682
42. K. Parvez, S. Yang, Y. Hernandez, A. Winter, A. Turchanin, X. Feng and K. Müllen, *ACS Nano*, 2012, **6**, 9541-9550.
43. H. Peng, Z. Mo, S. Liao, H. Liang, L. Yang, F. Luo, H. Song, Y. Zhong and B. Zhang, *Sci. Rep.*, 2013, **3**,1765
44. Z. Wen, S. Ci, Y. Hou and J. Chen, *Angew. Chem. Int. Ed.*, 2014, **53**, 6496-6500.
45. S. Stankovich, D. A. Dikin, R. D. Piner, K. A. Kohlhaas, A. Kleinhammes, Y. Jia, Y. Wu, S. T. Nguyen and R. S. Ruoff, *Carbon*, 2007, **45**, 1558-1565.
46. S. Yang, X. Feng, X. Wang and K. Müllen, *Angew. Chem.Int. Ed.*, 2011, **50**, 5339-5343.
47. S.-Y. Yang, K.-H. Chang, Y.-L. Huang, Y.-F. Lee, H.-W. Tien, S.-M. Li, Y.-H. Lee, C.-H. Liu, C.-C. M. Ma and C.-C. Hu, *Electrochem. Commun.*, 2012, **14**, 39-42.
48. R. Banerjee, A. Phan, B. Wang, C. Knobler, H. Furukawa, M. O'Keeffe and O. M. Yaghi, *Science*, 2008, **319**, 939-943.
49. W. Shi, X. Rui, J. Zhu and Q. Yan, *J. Phys. Chem. C*, 2012, **116**, 26685-26693.
50. O. Zhou, H. Shimoda, B. Gao, S. Oh, L. Fleming and G. Yue, *Acc. Chem. Res.*, 2002, **35**, 1045-1053.
51. X. Ji, K. T. Lee and L. F. Nazar, *Nat. Mater.*, 2009, **8**, 500-506.
52. Y. Zhao, K. Watanabe and K. Hashimoto, *J. Am. Chem. Soc.*, 2012, **134**, 19528-19531.
53. Q. Lin, X. Bu, A. Kong, C. Mao, X. Zhao, F. Bu and P. Feng, *J. Am. Chem. Soc.*, 2015, **137**, 2235-2238.
54. W. Wei, H. Liang, K. Parvez, X. Zhuang, X. Feng and K. Müllen, *Angew. Chem.*, 2014, **126**, 1596-1600.
55. J. Y. Cheon, T. Kim, Y. Choi, H. Y. Jeong, M. G. Kim, Y. J. Sa, J. Kim, Z. Lee, T.-H. Yang, K. Kwon, O. Terasaki, G.-G. Park, R. R. Adzic and S. H. Joo, *Sci. Rep.*, 2013, **3**,2715
56. C. W. B. Bezerra, L. Zhang, K. Lee, H. Liu, A. L. B. Marques, E. P. Marques, H. Wang and J. Zhang, *Electrochim. Acta*, 2008, **53**, 4937-4951.
57. A. Kong, Y. Kong, X. Zhu, Z. Han and Y. Shan, *Carbon*, 2014, **78**, 49-59.
58. F. Jaouen, E. Proietti, M. Lefevre, R. Chenitz, J.-P. Dodelet, G. Wu, H. T. Chung, C. M. Johnston and P. Zelenay, *Energ. Environ. Sci.*, 2011, **4**, 114-130.
59. Y. Nie, L. Li and Z. Wei, *Chem.Soc.Rev.*, 2015, **44**, 2168-2201.

View Article Online
DOI: 10.1039/C6TA00154H

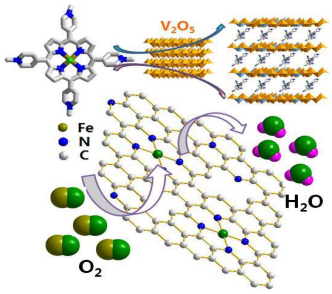

Few-layer porous porphyrinic carbon nanosheets with highly efficient oxygen electroreduction performance were obtained by thermal conversion of Fe-porphyrin/V_2O_5 intercalation compounds.